Pure appl. geophys. 157 (2000) 2047–2062
0033–4553/00/122047–16 $ 1.50 + 0.20/0

Pure and Applied Geophysics

Parallel 3-D Simulation of Ground Motion for the 1995 Kobe Earthquake: The Component Decomposition Approach

TAKASHI FURUMURA[1,*] and KAZUKI KOKETSU[2]

Abstract—A new approach to parallel pseudospectral simulation of 3-D seismic wave propagation is developed based on component decomposition of the wavefield. Field quantities and equations of motion are distributed over three processors according to their relationship to the x-, y- and z-coordinates, and computation is carried out concurrently on each processor with inter-processor communications. The efficiency of this approach is evaluated by a theoretical estimate and actual benchmark computations. We then conduct a 3-D simulation of strong ground motion for the 1995 Kobe (Hyogo-ken Nanbu) earthquake in order to show the feasibility of the parallel pseudospectral method. The results of the simulation demonstrate that the complex 3-D structures of the subsurface medium and source fault greatly affect the strong ground motion on the surface.

Key words: 1995 Kobe earthquake, parallel computing, pseudospectral method, strong ground motion, 3-D simulation.

Introduction

For large-scale 3-D modeling of seismic wave propagation, RESHEF *et al.* (1998) first attempted parallel Fourier pseudospectral computation using a CRAY X-MP supercomputer, and he has been followed by SATO *et al.* (1995), FURUMURA *et al.* (1998) and HUNG and FORSYTH (1998). In these studies the whole 3-D space is divided into subdomains, and the field quantities in each subdomain are assigned to each processor for concurrent computing. Instead of this domain partition approach, we can alternatively separate the x- y- and z-components of the field quantities and assign them to three processors separately.

We will present here a new parallel scheme of the pseudospectral method based on the component decomposition, with a brief overview of the 3-D wavefield calculation by the pseudospectral method. The efficiency of this parallel scheme will

---

[1] Hokkaido University of Education, Midorigaoka 2-34-1, Iwamizawa, 068-8642, Japan. E-mail: furumura@iwa.hokkyodai.ac.jp

[2] Earthquake Research Institute, University of Tokyo, Yayoi 1-1-1, Bunkyo-ku, 113-0032, Japan. E-mail: inquiry@taro.eri.u-tokyo.ac.jp

[*] Present address: Earthquake Research Institute, University of Tokyo, Yayoi 1-1-1, Bunkyo-ku, 113-0032, Japan. E-mail: furumura@eri.u-tokyo.ac.jp

be predicted by theoretical experiments, and complemented by actual computations. We then conduct a large-scale parallel 3-D simulation of strong ground motion for the 1995 Kobe (Hyogo-ken Nanbu) earthquake to demonstrate the feasibility of the component decomposition approach.

Pseudospectral Simulation of 3-D Wave Propagation

In a 3-D Cartesian coordinate system with the z-axis taken position downward, the equations of motion are represented as

$$\rho \ddot{u}_p = \frac{\partial \sigma_{xp}}{\partial x} + \frac{\partial \sigma_{yp}}{\partial y} + \frac{\partial \sigma_{zp}}{\partial z} + f_p, \quad (p = x, y, z), \tag{1}$$

where σ_{pq}, f_p and ρ stand for a stress, body force and density, respectively. $\ddot{u}_p$ is a particle acceleration, namely the second-order time derivative of a displacement. The stresses in an isotropic medium are given by

$$\sigma_{pq} = \lambda(e_{xx} + e_{yy} + e_{zz})\delta_{pq} + 2\mu e_{pq}, \quad (p, q = x, y, z), \tag{2}$$

with the Lamé's constants λ, μ and the strains defined by

$$e_{pq} = \frac{1}{2}\left(\frac{\partial u_p}{\partial q} + \frac{\partial u_q}{\partial p}\right), \quad (p, q = x, y, z). \tag{3}$$

Equation (1) is numerically integrated with the time step Δt as

$$\dot{u}_p^{n+1/2} = \dot{u}_p^{n-1/2} + \frac{1}{\rho}\left(\frac{\partial \sigma_{px}^n}{\partial x} + \frac{\partial \sigma_{py}^n}{\partial y} + \frac{\partial \sigma_{pz}^n}{\partial z} + f_p^n\right)\Delta t, \quad (p = x, y, z). \tag{4}$$

$\dot{u}_p^{n\pm 1/2}$ is a particle velocity at the time of $t = (n \pm \frac{1}{2})\,\Delta t$. The spatial derivatives in Equation (4) are calculated analytically in the wavenumber domain by use of the fast Fourier transform (FFT) (see e.g., FURUMURA *et al.*, 1998). Other spectral expansions based on the Chebyshev polynomials (e.g., KOSLOFF *et al.*, 1990) or the Legendre polynomials (e.g., FACCIOLI *et al.*, 1997; KOMATITSCH and VILOTTE, 1998) can be also used, that are superior in convergence properties and the handling of boundary conditions for highly complex underground structures.

The differentiation of Equations (2) and (3) with respect to time yields

$$\sigma_{pq}^{n+1} = \sigma_{pq}^n + \left[\lambda\left(\frac{\partial \dot{u}_x^{n+1/2}}{\partial x} + \frac{\partial \dot{u}_y^{n+1/2}}{\partial y} + \frac{\partial \dot{u}_z^{n+1/2}}{\partial z}\right)\delta_{pq} + \mu\left(\frac{\partial \dot{u}_p^{n+1/2}}{\partial q} + \frac{\partial \dot{u}_q^{n+1/2}}{\partial p}\right)\right]\Delta t, \quad (p, q = x, y, z). \tag{5}$$

The spatial derivatives in Equation (5) are again calculated in the wavenumber domain. The stresses at the next time step $t = (n + 1)\,\Delta t$ are then calculated by Equation (5) and the particle velocities resulting from Equation (4).

Component Decomposition

For parallel pseudospectral simulation of 3-D seismic wavefields, the domain partition approach, which divides the whole model into 2^N subregions and assigns them to processors, has usually been used (e.g., Sato *et al.*, 1995; Furumura *et al.*, 1998; Hung and Forsyth, 1998). However, if multiples of three processors are available, it is straightforward to partition the 3-D wavefield into three parts according to the closeness to the x-, y- and z-coordinates.

We first separate the nine equations of 3-D in Equations (4) and (5) into three groups. The x-component group consists of

$$\dot{u}_x^{n+1/2} = \dot{u}_x^{n-1/2} + \frac{1}{\rho}\left(\frac{\partial \sigma_{xx}^n}{\partial x} + \frac{\partial \sigma_{xy}^n}{\partial y} + \frac{\partial \sigma_{xz}^n}{\partial z}\right)\Delta t, \tag{6}$$

$$\sigma_{xx}^{n+1} = \sigma_{xx}^n + \left[(\lambda + 2\mu)\frac{\partial \dot{u}_x^{n+1/2}}{\partial x} + \lambda\left(\frac{\partial \dot{u}_y^{n+1/2}}{\partial y} + \frac{\partial \dot{u}_z^{n+1/2}}{\partial z}\right)\right]\Delta t, \tag{7}$$

$$\sigma_{xy}^{n+1} = \sigma_{xy}^n + \mu\left(\frac{\partial \dot{u}_x^{n+1/2}}{\partial y} + \frac{\partial \dot{u}_y^{n+1/2}}{\partial x}\right)\Delta t, \tag{8}$$

and the y-, z-component groups are

$$\dot{u}_y^{n+1/2} = \dot{u}_y^{n-1/2} + \frac{1}{\rho}\left(\frac{\partial \sigma_{xy}^n}{\partial x} + \frac{\partial \sigma_{yy}^n}{\partial y} + \frac{\partial \sigma_{yz}^n}{\partial z}\right)\Delta t, \tag{9}$$

$$\sigma_{yy}^{n+1} = \sigma_{yy}^n + \left[(\lambda + 2\mu)\frac{\partial \dot{u}_y^{n+1/2}}{\partial y} + \lambda\left(\frac{\partial \dot{u}_x^{n+1/2}}{\partial x} + \frac{\partial \dot{u}_z^{n+1/2}}{\partial z}\right)\right]\Delta t, \tag{10}$$

$$\sigma_{yz}^{n+1} = \sigma_{yz}^n + \mu\left(\frac{\partial \dot{u}_y^{n+1/2}}{\partial z} + \frac{\partial \dot{u}_z^{n+1/2}}{\partial y}\right)\Delta t, \tag{11}$$

and

$$\dot{u}_z^{n+1/2} = \dot{u}_z^{n-1/2} + \frac{1}{\rho}\left(\frac{\partial \sigma_{xz}^n}{\partial x} + \frac{\partial \sigma_{yz}^n}{\partial y} + \frac{\partial \sigma_{zz}^n}{\partial z}\right)\Delta t, \tag{12}$$

$$\sigma_{zz}^{n+1} = \sigma_{zz}^n + \left[(\lambda + 2\mu)\frac{\partial \dot{u}_z^{n+1/2}}{\partial z} + \lambda\left(\frac{\partial \dot{u}_x^{n+1/2}}{\partial x} + \frac{\partial \dot{u}_y^{n+1/2}}{\partial y}\right)\right]\Delta t. \tag{13}$$

$$\sigma_{xz}^{n+1} = \sigma_{xz}^n + \mu\left(\frac{\partial \dot{u}_x^{n+1/2}}{\partial z} + \frac{\partial \dot{u}_z^{n+1/2}}{\partial x}\right)\Delta t, \tag{14}$$

respectively.

If three processors called CPU-x, CPU-y, and CPU-z are available, these equation groups are assigned to them separately. The field quantities are also distributed over the three processors as $\dot{u}_x$, $\partial \dot{u}_x/\partial x$, σ_{xx}, and σ_{xy}, are assigned to CPU-x; $\dot{u}_y$, $\partial \dot{u}_y/\partial y$, σ_{yy}, and σ_{yz} to CPU-y, and $\dot{u}_z$, $\partial \dot{u}_z/\partial y$, σ_{zz}, and σ_{xz} to CPU-z. Each processor is responsible for the calculation of the corresponding equations, as well as performing interprocessor communications to obtain necessary quantities on the other processors. The material parameters λ, μ, ρ, and Q are commonly stored in the local memories of the three processor in a compressed form. They are arranged to be fit for a 3-D array of one-byte data, and retrieved directly through an index table.

Figure 1 illustrates how parallel computing is performed on a cluster of three processors by the component decomposition approach mentioned above. In the first stage of CPU-x, the derivatives $\partial\sigma^n_{xx}/\partial x$, and $\partial\sigma^n_{xy}/\partial y$ are calculated directly from quantities stored in the local memory. Message passing is then carried out to obtain σ^n_{xz} from CPU-z for computing $\partial\sigma^n_{xz}/\partial z$. The particle velocity $\dot{u}_x$ is then updated from $\dot{u}^{n-1/2}_x$ to $\dot{u}^{n+1/2}_x$ following Equation (6). In the second stage, CPU-x first calculates $\partial\dot{u}^{n+1/2}_x/\partial x$ using $\dot{u}^{n+1/2}_x$ in local memory. The processor then obtains $\partial\dot{u}^{n+1/2}_y/\partial y$ and $\partial\dot{u}^{n+1/2}_z/\partial z$ which have been calculated by CPU-y and CPU-z simultaneously, and updates the stress σ_{xx} from σ^n_{xx} to σ^{n+1}_{xx} following Equation (7). CPU-x finally receives $\dot{u}^{n+1/2}_y$ from CPU-y by message passing, and updates the stress σ_{xy} from σ^n_{xy} to σ^{n+1}_{xy} following Equation (8). Since we implement the above procedure by introducing standard Message Passing Interface (MPI; GROPP *et al.*, 1995), our code can run on a variety of platforms with few modifications.

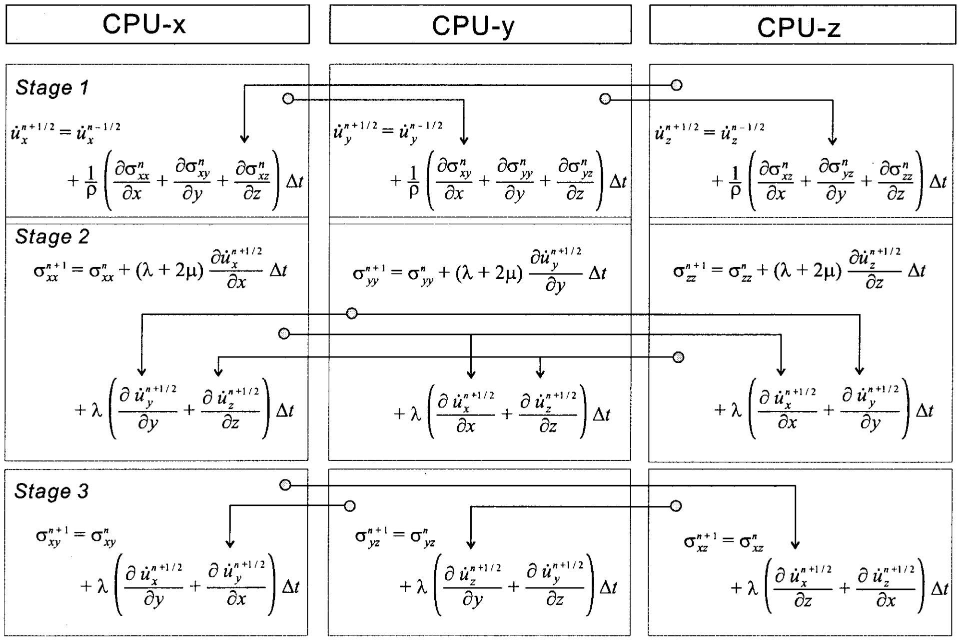

Figure 1

Diagram of the component decomposition for the parallel pseudospectral computing by the processors CPU-x, CPU-y, CPU-z. Each processor concurrently updates its corresponding particle velocity and stresses, and inter-processor communications indicated by arrows are required at each stage of the computation due to the coupling of the equations of motion over components. MPI is used for the inter-processor communications.

Efficiency of the Parallel Computation

If three processors are connected by an ideally fast network, the CPU time at each processor should be reduced to 1/3, and the speed-up rate by the parallel computation should approach 3. However, actual computer networks perform the communication only at a limited speed, compared with the computation speed of processors. We assume that the computation is carried out entirely in single-precision arithmetic for a 3-D model with $N_x \times N_y \times N_z$ grid points, and thus all the field quantities and their spatial derivatives occupy $N_x \times N_y \times N_z \times 4$ bytes. We further assume that the communication between each processor pair has the same communication speed V_c bytes/s, and no collisions occur during communications. The component decomposition approach requires twelve transmissions of quantities as shown in Figure 1. Therefore, the total communication time at each processor is given by

$$T_c = \frac{N_x \times N_y \times N_z \times 4}{V_c} \times 4, \tag{15}$$

if three transmissions can be performed concurrently by the three processors.

We define here the computation speed V_d as

$$V_d = \frac{N_x \times N_y \times N_z \times 4}{T_d}, \tag{16}$$

using the total CPU time T_d for the computation on a single processor. For a three-processor parallel system, the CPU time at each processor must be $T_d/3$, and thus we can roughly estimate the speed-up rate by

$$R = \frac{T_d}{T_d/3 + T_c} = \frac{3}{1 + 12V_d/V_c}. \tag{17}$$

We now implement the conventional pseudospectral code on a workstation with a DEC Alpha 21164A processor of 500 MHz and 1 Gbyte memory, and measure V_d for various model sizes. We then connected three such workstations using 100BaseT Ethernet, and measured V_c through a simple communication performance test of the MPI library. The results of these experiments showed that a cluster of workstations runs at around $V_d = 0.18$ Mbyte/s and $V_c = 6.2$ Mbyte/s. By inserting these values into Equation (17), we expect a peak speed-up rate of $R = 2.2$ for parallel computing using the cluster of three workstations. We note that R will approach to $2.7 \sim 2.8$ if we employ a much faster computer network such as 1000BaseT Ethernet which is at least three or four times faster than the 100BaseT system.

To compliment the theoretical estimate we next implement the component decomposition pseudospectral code on the three-workstation cluster, and measure

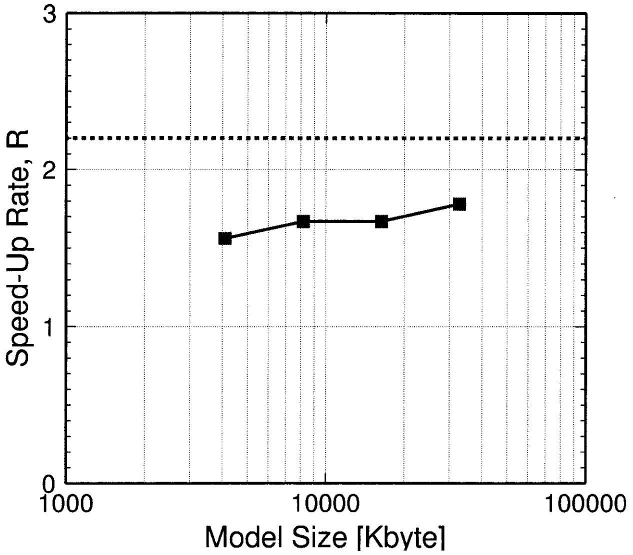

Figure 2
Experimental efficiency of the parallel 3-D pseudospectral computing using a cluster of three workstations with various model sizes. The dashed line indicates the theoretical peak performance rate of $R = 2.2$.

the actual speed-up rate relative to the single processor computation time for various model sizes. The result in Figure 2 indicates that the rate gradually increases from $R = 1.5$ to 1.8 as the model size increases. Although the rates are slightly lower than the theoretical peak rate, probably because of the overhead of MPI with small data size transmissions (GROPP *et al.*, 1995), we expect good performance rates for large-scale simulations.

The 1995 Kobe Earthquake

The 1995 Kobe earthquake (M_w 6.9) is the most damaging in recent Japanese history after the 1923 Kanto earthquake (M_s 8.2), and its notable feature is that most of the damage and over 6000 casualties occurred in the narrow zone called "damage belt." This 25 km-long belt extends through the City of Kobe with a width of about 2 km (gray zone in Fig. 3), and a source fault was assumed just beneath it at first (SHIMAMOTO, 1995), However, no fault with evidence of recent rupture has been found there by any geophysical survey, but the distribution of aftershocks and static displacements indicates the active strike-slip faults northwest of the belt (thick lines in Fig. 3) to be the source fault system of the earthquake (e.g., YOSHIDA *et al.*, 1996; SEKIGUCHI *et al.*, 1996).

Usually a fault-rupture propagation generates strong ground motions along the direction of propagation, and this directivity effect should be significant in fault-normal ground motions above the source fault system and beyond its leading end (KOKETSU, 1996; INOUE and MIYATAKE, 1997). The strong motion records in Figure 3 show the effect clearly. They mainly consist of two large, long-period ($1 \sim 2$ s) pulses, since two asperities of large slip occurred in the source fault system as recovered by YOSHIDA *et al.* (1996) (Fig. 4). However, the strong ground motion causing the severe damage is migrated from the source fault traces into the center of Kobe city as mentioned above, and consequently this migration should be due to the complex subsurface structure in Kobe. Simulations of ground motion have already been carried out by FURUMURA and KOKETSU (1998), PITARKA *et al.* (1998) and others (see chap. 5 IRIKURA *et al.*, 1999) for reproducing the migration.

Kobe forms the western half of the Osaka basin together with the Osaka bay. The basin is bounded on the north by the Rokko mountains, where the granite bedrock is exposed, and this boundary corresponds to the source fault system. The

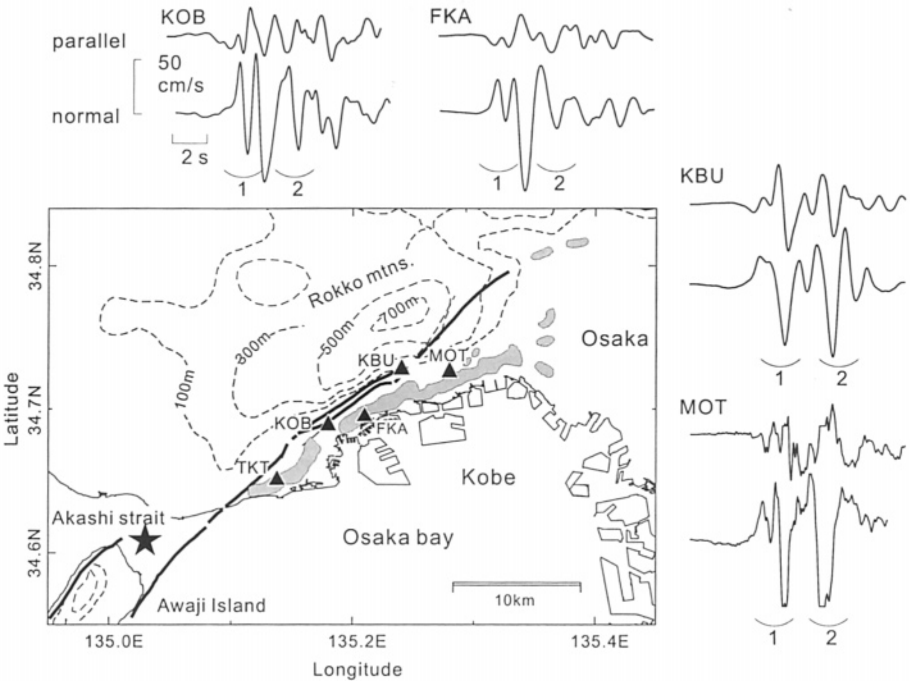

Figure 3

Index map of the 1995 Kobe (Hyogo-ken Nanbu) earthquake. The star symbol, gray zone and thick lines indicate the epicenter, damage belt and source faults, respectively. Dashed lines denote ground elevation. The fault rupture was initiated beneath the Akashi strait and propagated bilaterally towards Kobe and the Awaji island along known active fault traces. The seismograms on the top and right sides show the fault-parallel and fault-normal ground velocities recorded at the stations near the fault (note that the seismograms of MOT are clipped). The two large long-period pulses are numbered 1 and 2.

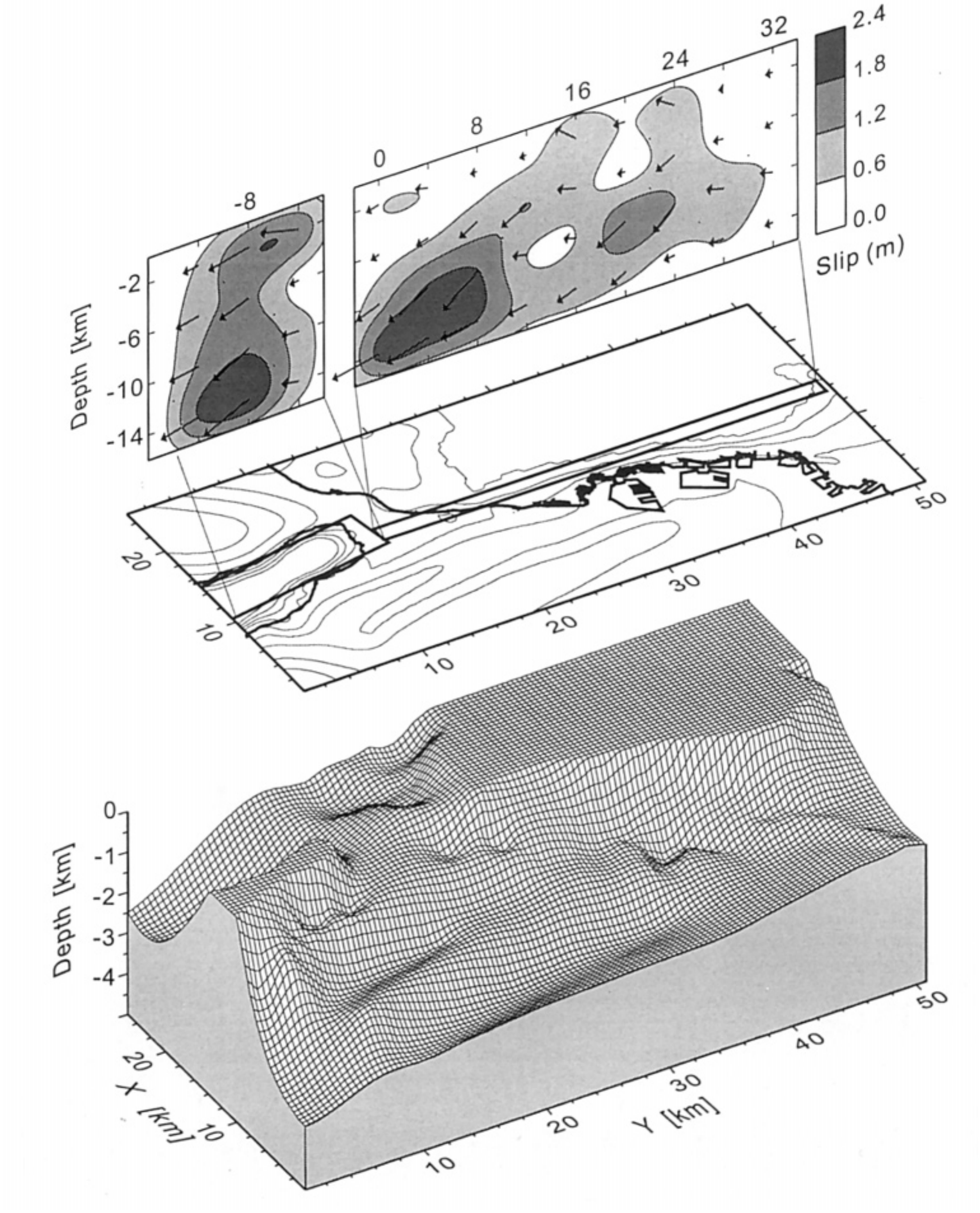

Figure 4
The topography of sediment/bedrock interface by NAKAGAWA *et al.* (1996) is shown by tthe contour drawing (middle) and in a bird's-eye view (bottom). The surface projections of the fault planes are also shown in the middle diagram. The top diagram represents the slip distribution recovered by YOSHIDA *et al.* (1996).

Table 1

Velocity model by KAGAWA *et al. (1993)*

	V_p (km/s)	V_s (km/s)	ρ (t/m^3)	Q
Sediment 1	1.6	0.35	1.7	60
Sediment 2	1.8	0.55	1.8	100
Sediment 3	2.5	1.0	2.1	150
Bedrock 1	5.4	3.2	2.7	300
Bedrock 2	6.0	3.46	2.8	500

thickness of the sediments rapidly changes from the mountains to the shoreline of the Osaka bay. A gentle slope then extends to the center of the bay, where the thickness is over 2500 m (Fig. 4; NAKAGAWA *et al.*, 1996). KAGAWA *et al.* (1993) derived very low S-wave velocities $0.35 \sim 1.0$ km/s for the sediments from refraction experiments (Table 1). The contrast between them and the velocity in the bedrock (3.2 km/s) should result in high amplification of seismic motions in the sediments. However, the previous simulations of the ground motion did not include the near-surface low-velocity layer of $V_s = 0.35$ km/s due to limitations of computer memory. We therefore carry out the simulation once again with this low-velocity layer by using the parallel pseudospectral method mentioned in the preceding sections.

3-D Ground Motion Simulation in Kobe

We employ a $51.2 \times 25.6 \times 40$ km model, which is discretized by a uniform grid spacing of 0.1 km in the horizontal directions. Variable grid spacing is applied in the vertical direction with intervals of 0.1 to 0.4 km by using the mapping technique of FORNBERG (1998). The area covered by this 3-D model is almost the same as that of our previous study (FURUMURA and KOKETSU, 1998), however the finer spacing results in 16.77 million grid points and the pseudospectral simulation with them requires 1.8 Gbyte memory, which is four times larger than that of the previous study. Even though we introduce the shallowest layer with $V_s = 0.35$ km/s, which was omitted in the previous study, the fine spacing allows us to simulate frequency components up to 1.75 Hz with at least 3.5 grid points per shortest S-wave wavelength.

In order to suppress artificial reflections and wraparound phases, the absorbing buffer zones of CERJAN *et al.* (1985) are applied along the outer limits with a width of twenty grid points. The boundary condition at the free surface is incorporated simply by introducing a zone of $\lambda = \mu = 0$ over the surface (“vacuum formulation”; see e.g., GRAVES, 1996). Since the vacuum formulation often causes the Gibbs phenomenon in case of a seismic source near the free surface, we use the “symmetric differentiation" technique (see FURUMURA and TAKENAKA, 1992 and FURUMURA *et al.*, 1998 for details).

We adopt the 3-D topography of the sediment/bedrock interface derived by NAKAGAWA *et al.* (1996) from gravity and reflection surveys, and the velocity model of KAGAWA *et al.* (1993) shown in Table 1. We assume the Q factors to be $60 \sim 50$ and $300 \sim 500$ in the sediments and bedrock, respectively. The anelastic attenuation is incorporated in the time integration procedure of Equations (4) and (5) by multiplying the stresses and velocities by the damping coefficients corresponding to the Q factors (GRAVES, 1996).

For the earthquake source, we adopt the fault model by YOSHIDA *et al.* (1996), whose slip distribution is shown in Figure 4 with the topography of the sediment/bedrock interface. Their model is represented by point dislocations at the centers of 4 by 4 km subfaults, and the fault slip is allowed to occur at each subfault in three successive time windows of length 1 s. The slip rate functions are approximated by HERRMANN's (1979) pseudo-delta function with a corner frequency of 1 Hz. To avoid spatial aliasing, the interval between the point sources must be shorter than the minimum wavelength of S-waves, so that we further divide each subfault into four smaller pieces, assigning linearly interpolated slip rate functions.

The 3-D parallel simulation takes 160 hours to complete the 22.5 s (5000 time steps) of ground motion using the cluster of three DEC Alpha workstations. Figure 5 displays the result of this simulation by snapshots of horizontal ground motion. In the first panel ($T = 6.3$ s), the first directivity pulse with amplitude over 50 cm/s is being generated from the asperity below western Kobe. The second pulse then begins to emerge from the second asperity below central Kobe in the $T = 8.6$ s panel. These two pulses are well developed and propagating to the east in the third panel of $T = 10.4$ s. The lower-right panel of Figure 5 illustrates the distribution of peak ground velocities of the horizontal motion during the entire duration of the simulation. This distribution reproduces the narrow belt of ground velocity larger than 60 cm/s. This zone extends over 20 km along the basin edge and nearly coincides with the damage belt in Figure 3.

Interpretation of the Simulation Results

Figure 6 compares the simulated fault-normal ground velocities with the observed seismograms at the near-fault stations TKT, KOB, FKA, KBU, and MOT (see Fig. 3). A band-pass filter has been applied to both the synthetics and observations with a frequency range between 0.1 to 1.75 Hz except for the clipped observation at MOT. Compared with the previous study (FURUMURA and KOKETSU, 1998), the two directivity pulses are reproduced more clearly by this simulation. In particular, the peak ground velocities at the basin stations (TKT, FKA) are considerably improved by the introduction of the 0.35 km/s layer.

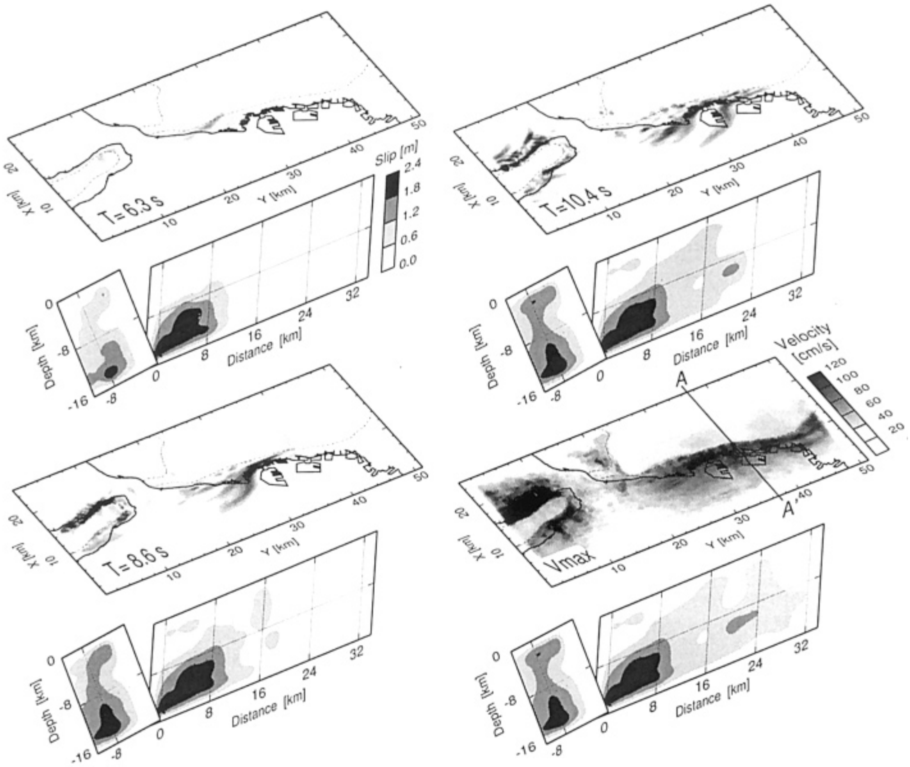

Figure 5
Snapshots of simulated horizontal ground velocities. The bottom-right panel $V_{\max}$ displays the distribution of peak ground velocities during the 22.5 s of the simulation. The dashed lines denote the basin edge. The progress of the fault rupture is also shown by snapshots.

However, they are still $60 \sim 80\%$ of the observed values, probably because the source model used does not include frequency components higher than 1 Hz. The discrepancy in the waveforms may be due to the variation of the shallowmost subsurface structure.

Figure 7 illustrates the simulated ground motions along the line A-A′ in Figure 5. The distribution of horizontal peak velocities along this line is also displayed in the uppermost panel of the figure. The two directivity pulses are significantly amplified by the propagation through the low-velocity sediments, and the second one produces large surface waves at the basin edge. We can see in the basin that the constructive interference between these surface waves and the direct *S*-wave propagating upward from the basin bottom enhances the ground velocity in the zone slightly away from the basin edge. This is called the “basin edge effect” (KAWASE, 1996; Pitarka *et al.*, 1996, 1998). The width of the damage belt and its distance from the basin edge is quite sensitive to the structure of the basin edge; wall angle, depth to the basin bottom, and the velocity contrast at the sediment/bedrock interface (Kawase *et al.*, 1998).

We note that the damage belt can also appear even when the source fault is distant from the basin edge. Figure 8(a) illustrates the peak horizontal velocities calculated for the fault that is located in the Rokko mountains 2 km from the basin edge. In the figure we again see the belt of large ground velocity in the basin, though the peak velocity is much smaller than that in Figure 6. In contrast, when the source fault is located below the basin, the zone appears just above the fault trace with a larger width, shorter length and higher amplitude (Fig. 8(b)). These results indicate that detailed knowledge of a 3-D subsurface structure and source fault geometry is indispensable to understand ground motions near a source fault.

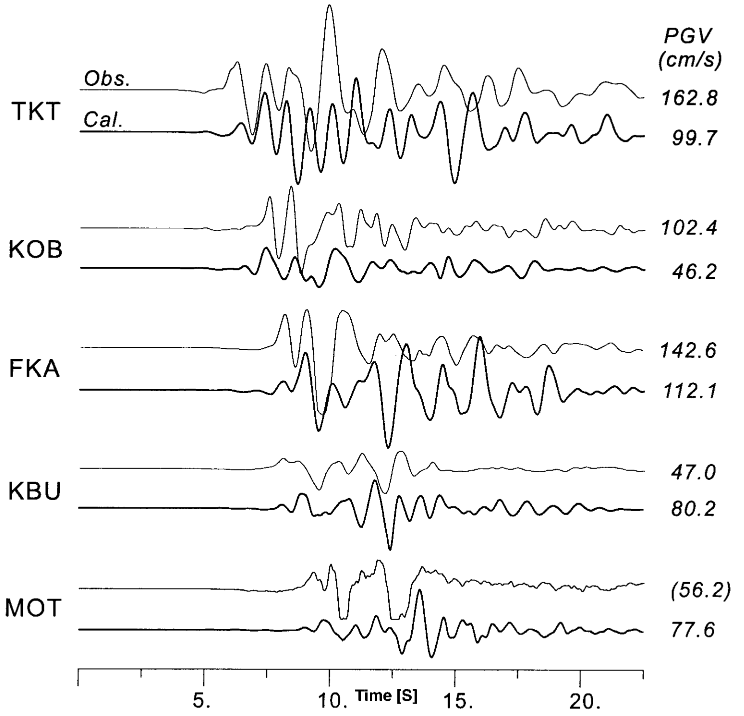

Figure 6
Comparison of the simulated (thick lines) and observed fault-normal seismograms (thin lines) at the five stations in Figure 3. The maximum amplitudes are shown on the right sides of the traces. A band-pass filter of 1.0–1.75 Hz has been applied to the seismograms except for the clipped observation at MOT.

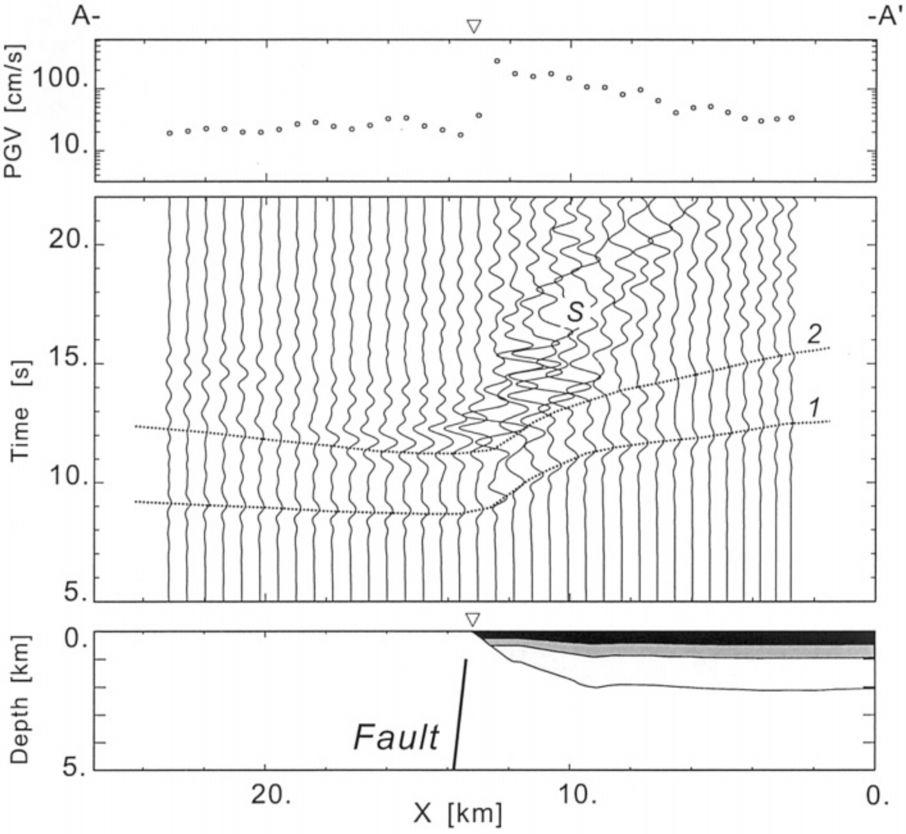

Figure 7

Sections of synthetic fault-normal motions (middle) and peak ground velocities (top) along the line A-A′ in Figure 5. The vertical profiles of the velocity model and source fault are also shown at the bottom. The direct *S*-wave fronts for the two directivity pulses are marked by the dashed lines and numbers 1, 2. *S* indicates surface waves generated at the basin edge.

Conclusions

We developed the component decomposition approach to the pseudospectral simulation of 3-D seismic wavefield, and applied it to the strong motion simulation of the 1995 Kobe earthquake with a realistic subsurface model in Kobe. We have successfully reproduced the strong ground shaking during the earthquake.

Numerical modeling of 3-D seismic wavefield has long been expensive and its application is restricted to rather long-period components of the wavefield due to the limitation of computer memory, except for a few pioneering studies using massively parallel computers. However, the component decomposition approach to the parallel pseudospectral simulation has realized a practical 3-D simulation by using only desktop workstations. This approach is not restricted to a system of

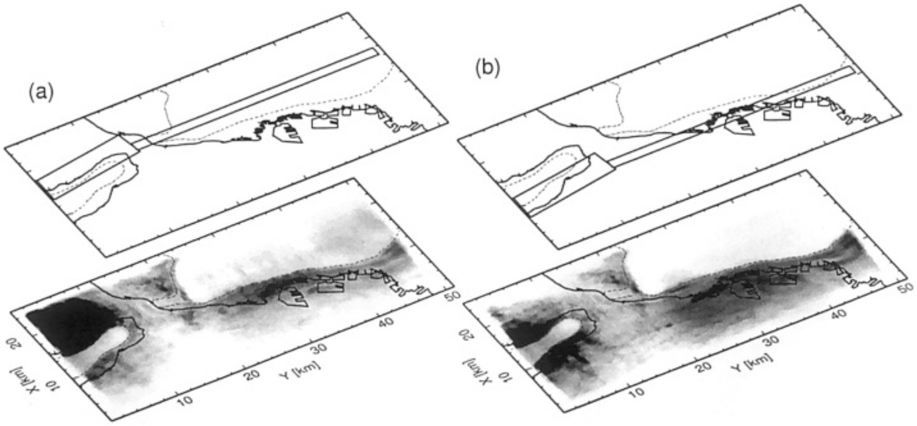

Figure 8
Distribution of peak ground velocities of horizontal motion for (a) the source fault 2 km from the actual location (Fig. 4) to the mountain range, and (b) that 2 km from the center of the basin.

three processors, but feasible for a massively parallel system of 3×2^N processors if we combine the approach with the domain partition scheme (e.g., FURUMURA *et al.*, 1998).

Acknowledgements

This study was supported by grants from the Japanese Ministry of Education, Science and Culture (Nos. 11115202 and 10740213) and the Earth Simulator Project of the Science and Technology Agency of Japan. We thank the Japan Meteorological Agency, Committee of Earthquake Observation Research in Kansai, Osaka Gas and Japan Railway (NAKAMURA *et al.*, 1996; No. R-036) for providing us with strong motion data. We gratefully acknowledge constructive comments by R. Madariaga, P. Mora and two anonymous reviewers.

REFERENCES

CERJAN, C., KOSLOFF, D., KOSLOFF, R., and RESHEF, M. (1985), *A Nonreflecting Boundary Condition for Discrete Acoustic and Elastic Wave Equations*, Geophysics *50*, 705–708.

FACCIOLI, E., MAGGIO, F., PAOLUCCI, R., and QUARTERONI, A. (1997), *2D and 3D Elastic Wave Propagation by a Pseudospectral Domain Decomposition Method*, J. Seismol. *1*, 237–251.

FORNBERG, B. (1998), *The Pseudospectral Method: Accurate Representation of Interfaces in Elastic Wave Calculations*, Geophysics *53*, 625–637.

FURUMURA, T., and TAKENAKA, H. (1992), *A Stable Method for Numerical Differentiation of Data with Discontinuities at End-points by Means of Fourier Transform-symmetric Differentiation*, Butsuri-tansa (J. SEGJ) *45*, 303–309 (in Japanese).

FURUMURA, T., KENNETT, B. L. N., and TAKENAKA, H. (1998), *Parallel 3-D Pseudospectral Simulation of Seismic Wave Propagation*, Geophysics *63*, 279–288.

FURUMURA, T., and KOKETSU, K. (1998), *Specific Distribution of Ground Motion During the 1995 Kobe Earthquake and its Generation Mechanism*, Geophys. Res. Lett. *25*, 785–788.

GRAVES, R. W. (1996), *Simulating Seismic Wave Propagation in 3D Elastic Media Using Staggered-grid Finite Differences*, Bull. Seismol. Soc. Am. *86*, 1091–1106.

GROPP, W., LUSK, E., and SKJELLUM, A., *Using MPI, Portable Parallel Programming with the Message-passing Interface* (The MIT Press, London 1995).

HERRMANN, R. B. (1979), *SH-wave Generation by Dislocation Source—A Numerical Study*, Bull. Seismol. Soc. Am. *69*, 1–15.

HUNG, S.-H., and FORSYTH, D. W. (1998), *Modeling Anisotropic Wave Propagation in Oceanic Inhomogeneous Structures Using the Parallel Multidomain Pseudospectral Method*, Geophys. J. Int. *133*, 726–740.

INOUE, T., and MIYATAKE, T. (1997), *3-D Simulation of Near-field Strong Motion: Basin Edge Effect Derived from Rupture Directivity*, Geophys. Res. Lett. *24*, 905–908.

IRIKURA, K., KUDO, K., OKADA, H., and SASATANI, T., *The Effects of Surface Geology on Seismic Motion, Volume 3* (A. A. Balkema, Rotterdam 1999).

KAGAWA, T., SAWADA, S., IWASAKI, Y., and NANJO, A. (1993), *Modeling of Deep Sedimentary Structure of the Osaka Basin*, Proc. 22th Earthq. Eng. Symp., 192–202 (in Japanese).

KAWASE, H. (1996), *The Cause of the Damage Belt in Kobe: "The Basin-edge Effect," Constructive Interference of the Direct S-wave with the Basin-induced Diffracted/Rayleigh Waves*, Seism. Res. Lett. *67*, 25–34.

KAWASE, H., MATSUSHIMA, S., GRAVES, R. W., and SOMERVILLE, P. G. (1998), *Three-dimensional Wave Propagation Analysis of Simple Two-dimensional Basin Structure with Special Reference to "the Basin-edge Effect"—The Cause of the Damage Belt during the Hyogo-ken Nanbu Earthquake*, Zisin *50*, 431–449 (in Japanese).

KOKETSU, K. (1996), *Damaging Californian Earthquakes and the 1995 Hyogo-ken Nanbu Earthquake*, Kagaku *66*, 93–97 (in Japanese).

KOMATITSCH, D., and VILOTTE, J.-P. (1998), *The Spectral Element Method: An Efficient Tool to Simulate the Seismic Response of 2D and 3D Geological Structures*, Bull. Seismol. Soc. Am. *88*, 368–392.

KOSLOFF, D., KESSLER, D., FILHO, A. Q., TESSMER, E., BEHLE, A., and STRAHILEVITZ, R. (1990), *Solution of the Equations of Dynamic Elasticity by a Chebyshev Spectral Method*, Geophysics *55*, 734–748.

NAKAGAWA, K., SHIONO, K., INOUE, N., and SANO, M. (1996), *Geological Characteristics and Problems in and Around Osaka Basin as a Basis for Assessment of Seismic Hazards*, Soil and Foundations, *Special Issue*, 15–28.

NAKAMURA, Y., UEHAN, F., and INOUE, H. (1996), *Waveform and its Analysis of the 1995 Hyogo-Ken-Nanbu Earthquake (II)*, JR Earthquake Information *23d*, Railway Technical Research Institute, 112 pp. (in Japanese).

PITARKA, A., IRIKURA, K., IWATA, T., and KAGAWA, K. (1996), *Basin Structure Effects in the Kober Area Inferred from the Modeling of Ground Motions from two Afterscocks of the January 17, 1995 Hyogoken-nanbu Earthquake*, J. Phys. Earth *44*, 563–576.

PITARKA, A., IRIKURA, K., IWATA, T., and SEKIGUCHI, H. (1998), *Three-dimensional Simulation of the Near-fault Ground Motion for the 1995 Hyogo-Ken Nanbu (Kobe), Japan, Earthquake*, Bull. Seismol. Soc. Am. *88*, 428–440.

RESHEF, M., KOSLOFF, D., EDWARDS, M., and HSIUNG, C. (1998), *Three-dimensional Elastic Modeling by the Fourier Method*, Geophysics *53*, 1184–1193.

SATO, T., MATSUOKA, T., and TSURA, T. (1995), Wavefield Modeling by Pseudospectral Method on a Parallel Computer (2) Seismic Data Simulation and Processing, Proc. SEGJ Conference *92*, 392–396 (in Japanese).

SEKIGUCHI, H., IRUKURA, K., IWATA, T., KAKEHI, Y., and HOSHIBA, M. (1996), *Minute Locating of Faulting beneath Kobe and the Waveform Inversion of the Source Process during the 1995 Hyogo-ken Nanbu, Japan, Earthquake Using Strong Ground Motion Records*, J. Phys. Earth *44*, 473–487.

SHIMAMOTO, T. (1995), *Earthquake Disasters in Kobe and Presumed Earthquake—Generating Faults*, Kagaku *65*, 195–198 (in Japanese).

YOSHIDA, S., KOKETSU, SHIBAZAKI, B., SAGIYA, T., KATO, T., and YOSHIDA, Y. (1996), *Joint Inversion of Near- and Far-field Waveforms and Geodetic Data for the Rupture Process of the 1995 Kobe Earthquake*, J. Phys. Earth *44*, 437–454.

(Received August 14, 1999, revised March 20, 2000, accepted April 10, 2000)